Original Article

MOLECULAR METABOLISM

# Elucidating the role of *Rgs2* expression in the PVN for metabolic homeostasis in mice

**Yue Deng [1], Jacob E. Dickey [1], Kenji Saito [1], Guorui Deng [1], Uday Singh [1], Jingwei Jiang [1], Brandon A. Toth [1], Zhiyong Zhu [2], Leonid V. Zingman [2,5], Jon M. Resch [1,5,6], Justin L. Grobe [3,4], Huxing Cui [1,5,6,*]**

## ABSTRACT

**Objective:** RGS2 is a GTPase activating protein that modulates GPCR-$G_\alpha$ signaling and mice lacking RGS2 globally exhibit metabolic alterations. While RGS2 is known to be broadly expressed throughout the body including the brain, the relative contribution of brain RGS2 to metabolic homeostasis remains unknown. The purpose of this study was to characterize RGS2 expression in the paraventricular nucleus of hypothalamus (PVN) and test its role in metabolic homeostasis.

**Methods:** We used a combination of RNAscope in situ hybridization (ISH), immunohistochemistry, and bioinformatic analyses to characterize the pattern of *Rgs2* expression in the PVN. We then created mice lacking *Rgs2* either prenatally or postnatally in the PVN and evaluated their metabolic consequences.

**Results:** RNAscope ISH analysis revealed a broad but regionally enriched *Rgs2* mRNA expression throughout the mouse brain, with the highest expression being observed in the PVN along with several other brain regions, such as the arcuate nucleus of hypothalamus and the dorsal raphe nucleus. Within the PVN, we found that *Rgs2* is specifically enriched in $CRH^+$ endocrine neurons and is further increased by calorie restriction. Functionally, although Sim1-Cre-mediated prenatal deletion of *Rgs2* in PVN neurons had no major effects on metabolic homeostasis, AAV-mediated adult deletion of *Rgs2* in the PVN led to significantly increased food intake, body weight (both fat and fat-free masses), body length, and blood glucose levels in both male and female mice. Strikingly, we found that prolonged postnatal loss of *Rgs2* leads to neuronal cell death in the PVN, while rapid body weight gain in the early phase of viral-mediated PVN *Rgs2* deletion is independent of PVN neuronal loss.

**Conclusions:** Our results provide the first evidence to show that PVN *Rgs2* expression is not only sensitive to metabolic challenge but also critically required for PVN endocrine neurons to function and maintain metabolic homeostasis.



**Keywords** Regulator of G protein signaling 2; Paraventricular nucleus of hypothalamus; Obesity; Food intake; Energy balance

## 1. INTRODUCTION

Substantial evidence indicates that the majority of genes linked to obesity [1] are abundantly expressed in the central nervous system (CNS), and functional investigations of those obesity-associated genes in animal models further support that the CNS, in particular the hypothalamus, is essential for metabolic homeostasis [2–4]. Accordingly, most of the current FDA-approved anti-obesity medications are known to act through the CNS to suppress food intake and/or promote energy expenditure [5]. Among many functionally distinct hypothalamic nuclei, the paraventricular nucleus of hypothalamus (PVN) has been considered a key integrative center in the brain for maintaining metabolic homeostasis through its projections to different hypothalamic and brainstem nuclei that regulate energy intake and/or expenditure [6–8]. A variety of G-protein-coupled receptors (GPCRs) involved in metabolic control are enriched in the PVN [9], such as melanocortin 4 receptor (MC4R), glucagon-like peptide 1 receptor (GLP1R), and various subtypes of serotonergic and adrenergic receptors, and functional manipulations of different $G_\alpha$ subunits within the PVN cause metabolic alterations [10,11], indicating a critical role of PVN GPCR-$G_\alpha$ signaling pathways in whole-body energy metabolism. However, the regulatory components of PVN GPCR-$G_\alpha$ signaling pathways affecting metabolic homeostasis are not well understood.

Regulators of G protein signaling (RGS) proteins are key modulators of GPCR-$G_\alpha$ signaling by acting as GTPase-activating proteins (GAP) to turn off $G_\alpha$ signal transduction upon GPCR activation [12]. RGS2 belongs to B/R4 RGS family members and is known to directly bind to and inhibit $G_{\alpha q}$ and $G_{\alpha i}$ through its GAP activities [13,14], or indirectly inhibit $G_{\alpha s}$ signaling by directly binding to and inhibiting the activity of adenylyl cyclase [15]. Functionally, RGS2 has been implicated in a variety of behavioral and physiological regulations, including emotional behaviors, cardiovascular control as well as metabolic homeostasis, as global *Rgs2* knockout ($Rgs2^{null}$) mice exhibit increased anxiety and fear behavior, autonomic dysfunction, elevated blood pressure, reduced

[1]Department of Neuroscience and Pharmacology, University of Iowa Carver College of Medicine, Iowa City, IA, United States [2]Department of Internal Medicine, University of Iowa Carver College of Medicine, Iowa City, IA, United States [3]Department of Physiology, Medical College of Wisconsin, Milwaukee, WI 53226, USA [4]Comprehensive Rodent Metabolic Phenotyping Core, Medical College of Wisconsin, Milwaukee, WI 53226, USA [5]Iowa Neuroscience Institute, University of Iowa Carver College of Medicine, Iowa City, IA, United States [6]F.O.E. Diabetes Research Center, University of Iowa Carver College of Medicine, Iowa City, IA, United States

*Corresponding author. Department of Neuroscience and Pharmacology, University of Iowa Carver College of Medicine, 51 Newton Road, 2-372 Bowen Science Building, Iowa City, IA 52242. Tel.: +319 335-6954; fax: +319 335-8930. E-mail: huxing-cui@uiowa.edu (H. Cui).

Received September 23, 2022 • Revision received October 9, 2022 • Accepted October 21, 2022 • Available online 25 October 2022

https://doi.org/10.1016/j.molmet.2022.101622

 

body weight, and impaired adipogenesis [16–21]. Consistent with this broad spectrum of functionalities, RGS2 is widely expressed throughout the body, including but not limited to, the brain, kidney, vasculature, heart, and adipose tissue. In the rat brain, it has been reported that *Rgs2* mRNA is highly expressed in the PVN along with other brain regions [22], yet the functional role of PVN RGS2 in the homeostatic regulation of energy balance remains unexplored. Here, we report that *Rgs2* mRNA is enriched in PVN CRH $^{+}$ endocrine neurons and caloric restriction further upregulates PVN *Rgs2* expression in mice. Viral-mediated postnatal, but not prenatal, deletion of *Rgs2* in the PVN results in significantly increased food intake and body weight, altered body composition, and impaired glucose homeostasis. In addition, we also show that prolonged postnatal deletion of *Rgs2* can lead to the death of PVN neurons. Overall, our results provide the first evidence to support the role of PVN RGS2 in the regulation of whole-body energy metabolism.

## 2. METHODS

### 2.1. Animals

Floxed *Rgs2* (*Rgs2*$^{f/f}$) mice were generated through the University of Iowa Genome Editing Facility by CRISPR/Cas9 insertion of two loxP sites flanking exons 2–4 of *Rgs2* gene as reported previously [23]. These newly generated *Rgs2*$^{f/f}$ mice have also been deposited to Jackson Laboratories (stock number: 037,619). Female *Rgs2*$^{f/f}$ mice were crossed with male *Sim1*-Cre mice (The Jackson Laboratory, stock #006395) to generate *Rgs2*$^{Sim1-KO}$ mice. Mice used in the present study were all maintained in B6/SJL mixed backgrounds. Animals were housed on 12 h light and dark cycle (lights on 06:00, Light off 18:00) at 20°C–24 °C, having ad libitum access to standard chow food (Envigo, #7913) or high-fat-high-sucrose diet (58 kcal% fat, Research Diet Incorporated, #D09071702) and water, unless indicated otherwise. Both sexes were used in the studies, unless otherwise specified. All animal protocols were approved by the Institutional Animal Care and Use Committee of the University of Iowa.

### 2.2. Antibodies and recombinant adeno-associated virus (AAV) constructs

Commercially available primary and secondary antibodies used in this study are as follows: anti-fluorogold (rabbit, Millipore #AB153); anti-CRH, (guinea pig, Peninsula Lab #T-5007); Donkey-anti-rabbit IgG (H + L) Alexa Fluor 594 (Jackson IR #711-585-152); Donkey-anti-guinea pig IgG Cy3 (Jackson IR #706-165-148).

Two sets of AAV-GFP and AAV-Cre-GFP from different vendors were used in the present study to achieve conditional *Rgs2* deletion in the PVN and independently confirm metabolic phenotypes. One set of AAV2-CMV-GFP ($5.9 \times 10^{12}$ vg/mL) and AAV2-CMV-Cre-GFP ($4.4 \times 10^{12}$ vg/mL) were purchased from the UNC viral vector core and another set of AAV2-CMV-eGFP (Addgene 105,530, $1.4 \times 10^{13}$ vg/mL, diluted to $7 \times 10^{12}$ vg/mL upon injection) and AAV2-CMV-eGFP-Cre (Addgene 105,545, $1.3 \times 10^{13}$ vg/mL, diluted to $6.5 \times 10^{12}$ vg/mL upon injection) were purchased from Addgene.

### 2.3. Stereotaxic surgery

Stereotactic surgery was performed as previously described [24,25]. Briefly, mice were anesthetized by intraperitoneal injection of ketamine/xylazine (100:10 mg/kg) and placed on a Kopf stereotaxic apparatus. Following standard disinfection procedure, ~1.0 cm incision was made to expose the skull of the mice and a small hole was drilled into the skull bilaterally at defined positions to target the PVN (coordinates: AP -0.8 mm, ML +1.1 mm, DV -4.9 mm with 10-degree injection arm). Pulled glass micropipette filled with a viral vector was slowly inserted to reach the targeted brain region and a small volume (200–250 nL) of injection was made by applying pulse pressure using Tritech pressure Microinjector (Tritech Research). After 10 min of waiting to ensure full penetration of the injectant into the targeted area, the needle was slowly removed, and the incision was closed by applying tissue glue and wound clips. The mice were then kept on a warming pad until awake and fed a regular chow diet throughout the experimental period unless otherwise noted. At least 4 weeks were given for animals to recover from surgery and to complete viral-mediated genetic recombination before performing any functional experiments. At the end of the study, all mice that received AAV injection were transcardially perfused with 10% neutralized formalin and the brains were processed for histological verification of correct stereotaxic targeting. Off-target cases were excluded from the final data analysis.

### 2.4. Quantitative polymerase chain reaction (qPCR)

Micro punches (diameter = 0.5 mm) of PVN from fresh-frozen brains of *Rgs2*$^{f/f}$ and *Rgs2*$^{Sim1-KO}$ mice were rapidly collected, snap frozen in liquid nitrogen, and kept at −80° until further processing. mRNA purification (RNeasy Plus Mini Kit, Qiagen #74134) and first strand cDNA preparation (iScript Reverse Transcription Supermix, Bio-rad #1708840) were performed as per the manufacturer's instructions. qPCR for *Rgs2* was performed with two primer pairs encompassing either exon 1–5 (forward 5′-TGGACAAGAGTGCAGGCAA; reverse 5′-TTCTGAGCTGTGGTGAAGCAG) or exon 2–4 (forward 5′-TCTTGCAGAATTCCTCTGCTC; reverse 5′-GCAGCCAGCCCATATTTACTG) of *Rgs2* gene using an Applied Biosystems StepOnePlus system. *Rgs2* expression was normalized to housekeeping gene *Ppia* (forward 5′-TGGAGAGCACCAAGACAGACA; reverse 5′-TGCCGGAGTCGACAATGAT) using the ΔΔCt method [26]. The PCR products of primer pair encompassing *Rgs2* exon 1–5 were run through gel electrophoresis to identify the existence of truncated *Rgs2* mRNA lacking exon 2–4 (Figs. S2B–E). The expression levels of other RGS genes (*Rgs4*, *Rgs5*, *Rgs7*, *Rgs10*, *Rgs12*, *Rgs17*) were determined exactly as in our previous publication [27].

### 2.5. In silico analysis of PVN single-cell RNA-seq data

Pre-processed data from single-cell RNA-seq of cells from the PVN was obtained from the NCBI GEO database (GSE148568) [28]. Data were imported, normalized, analyzed, and plotted using the R package Seurat 4.0 [29]. Briefly, after loading the data, Seurat objects were created followed by the "SCTransform" function to normalize, scale, and obtain variable features (3000). A resolution of 1.6 and 30 principal component dimensions were used to perform clustering analysis using the functions "RunUMAP", "FindNeighbors", and "FindClusters." After the initial analysis, three small *Sim1*-negative clusters and one small cluster comprised of low complexity cells were removed. The remaining 766 PV N neurons were reclustered using SCTransform as above.

### 2.6. Measurement of body weight and body length

For *Rgs2*$^{f/f}$ and *Rgs2*$^{Sim1-KO}$ mice, body weights were measured weekly throughout the study (starting from 4-week-old) with a digital scale. For *Rgs2*$^{f/f}$ and wild-type (WT) mice that received microinjection of AAVs into the PVN at age of 8 weeks, body weights were measured weekly throughout the study. For *Rgs2*$^{f/f}$ and WT mice that received microinjection of AAVs into the PVN at age of 18 weeks, body weights were measured at the time of surgery and then after 4 weeks of post-surgery. Mice were group housed throughout the study, except few short time windows during which single housing is required for

 

experimental need (food intake, locomotor activity, and metabolic cage study). For all the animals, the body length (crown-rump length) was measured from the tip of the nose to the end of the fur line on the tail under anesthesia at ~25-week-old.

### 2.7. Food intake

For home cage food intake and metabolic cage studies, animals were singly housed with free access to chow food (3.1 kcal/g, Envigo #7913) or high-fat-high-sucrose food (5.5 kcal/g, Research Diets #D09071702). After 3 days of acclimation, the daily food intake was measured manually for 3 days by weighing the remaining food pellets [30]. For Feeding Experimentation Device 3 (FED3, Open-ephys) studies, animals were group-housed overnight in customized FED3-attached home cages [25] to habituate for the fixed ratio 1 (FR1) protocol (one correct nose poke delivers one 20 mg food pellet, 3.35 kcal/g, Bio-Serv #F0163) and then singly housed continuously in FED3-attached home cages for additional 2 days to ensure each mouse is fully trained for FR1. Real-time consumption of food pellets was then recorded by FED3 for consecutive 3 days to evaluate daily food intake. Daily energy intake (kcal) was then calculated by daily food intake (g) × energy density (kcal/g).

### 2.8. General locomotion and drinking behavior

The locomotor activity and drinking behavior were measured using a Model 3000 Noldus PhenoTyper chamber (Noldus) as previously described [25]. Shredded paper bedding was provided on the floor (30 × 30 cm) to mimic a home cage-like environment. Animals were individually housed and acclimated overnight in the chamber and then continuously monitored for a complete light—dark cycle (24 h) with free access to food and water. During the experiment period, animal movement was tracked with an infrared CCD camera that connected to a desktop computer. The video data were processed in real-time with EthoVision XT 15 software (Noldus) to determine the total distance moved (cm). A lickometer was attached to the water bottle nozzle, and the licking counts were recorded to quantify drinking behavior.

### 2.9. Body composition

Body composition was determined using a nuclear magnetic resonance (NMR)-based minispec body composition analyzer (Minispec LF50, Bruker) located in the Metabolic Phenotyping Core Facility at the University of Iowa. Briefly, animals were restrained in a minispec probe after body weight measurement, and the probe was inserted into the instrument for the analysis of fat tissue, lean tissue, and free fluid. Animals were removed from the restrainer and returned to the home cage once data were acquired. Fat mass and fat-free mass were presented as the weight in gram (g) [31].

### 2.10. Energy expenditure (EE) and respiratory exchange ratio (RER)

Mice EE and RER were measured using the OxyMax/Comprehensive Lab Animal Monitoring System (CLAMS, Columbus Instruments) as previously described [32]. Animals were individually housed and acclimatized for a day in metabolic chambers, followed by a 2-day experimental period, with free access to food and water. Rates of $O_2$ consumption, $CO_2$ production, and locomotor activity were continuously recorded throughout the experimental period. Final data were presented as hourly bins as well as light—dark circadian cycles averaged from the 2-day experimental period.

### 2.11. Fed and fasting glucose levels

Before the experiment, animals were transferred to clean cages with fresh bedding and food was removed from the cages. Fed glucose level was measured after 2 h of food removal. Briefly, a small cut was made at the distal end of the tail to acquire a drop of blood. Blood glucose was then determined with a glucose meter (Freedom Lite, Abbott) and disposable glucose strips (Abbott). Fasting glucose was measured after 24 h of food removal.

### 2.12. Core body temperature

Rectal thermometry was performed to determine the core body temperature of the mice. Briefly, a temperature-sensitive probe (Auber-WS) was lubricated with mineral oil and gently inserted into the anus of the animal (~1.5 cm deep). The core temperature was taken once the reading from the probe became stable (usually ~10 s after insertion).

### 2.13. Plasma collection and corticosterone measurement

Mouse was placed in a restrainer and a small cut was made on the distal end of tail immediately to collect small volume of blood (baseline) using glass capillaries. Mouse was then continuously kept in the restrainer for additional 30 min and small volume of blood was collected again (stressed condition) from the tail using same method. Collected blood in the glass capillary was immediately transferred to an EDTA-treated tube followed by centrifugation at 2000G for 10 min at 4 °C. The supernatant was transferred to a new tube and centrifuged again at 10000G for 10 min at 4 °C, and the clear supernatant (plasma) was collected and stored at −80 °C till further process. All the samples were collected between 7:00—9:00 AM. The plasma corticosterone level was measured by Vanderbilt Hormone Assay & Analytical Service Core using radioimmunoassay kit (MP Biomedicals, #0712010-CF).

### 2.14. Tissue collection

Mice were transcardially perfused with cold phosphate-buffered saline (PBS) followed by 10% neutralized formalin for fixation. The brains were quickly dissected and post-fixed with 10% neutralized formalin overnight, cryopreserved in 25% sucrose solution at 4 °C overnight, and then cut into five series of 30 μm sections with a sliding microtome (SM2010 R, Leica). Brain sections were then stored in cryoprotectant (20% glycerol, 30% ethylene glycol, 50% PBS) at −20 °C until further processing.

### 2.15. Intraperitoneal fluorogold (FG) injection

Labeling of PVN endocrine neurons by intraperitoneal (i.p.) Fluorogold injection was conducted by following well-validated protocols described before [33—36]. Briefly, 60 μl of 2% FG stock aliquots were diluted in phosphate-buffered saline (PBS, Ph 7.4) to a total injection volume of 300 μl (final w/v concentration was 0.4% FG). Freshly prepared 0.4% Fluorogold solution was then injected into the intraperitoneal space of adult male C57BL/6 J mice. Animals were given one week for retrograde labeling of PVN endocrine neurons by FG before transcardiac perfusion. Immunohistochemistry of FG was performed as described below.

### 2.16. RNAScope in situ hybridization (ISH)

Detection of *Rgs2* mRNA was achieved by *in situ* hybridization with *Rgs2* RNAscope probe (Mm-Rgs2, ACD Bio #492931) and detection kits (RNAscope 2.5 HD Detection Reagent — Brown, ACD Bio #322310; RNAscope Fluorescent Multiplex Detection Reagents, ACD Bio #320851). Briefly, 10% neutralized formalin-fixed brain sections were washed in PBS and mounted on microscope slides (Superfrost Plus, Fisher Scientific #12-550-15), air-dried overnight at −20 °C, followed by standard hybridization protocols described in the manufacturer's instructions. For RNAscope 2.5 HD Brown assays, slides were mounted and coverslipped with DPX mountant (VWR, 100,503). For RNAscope

 

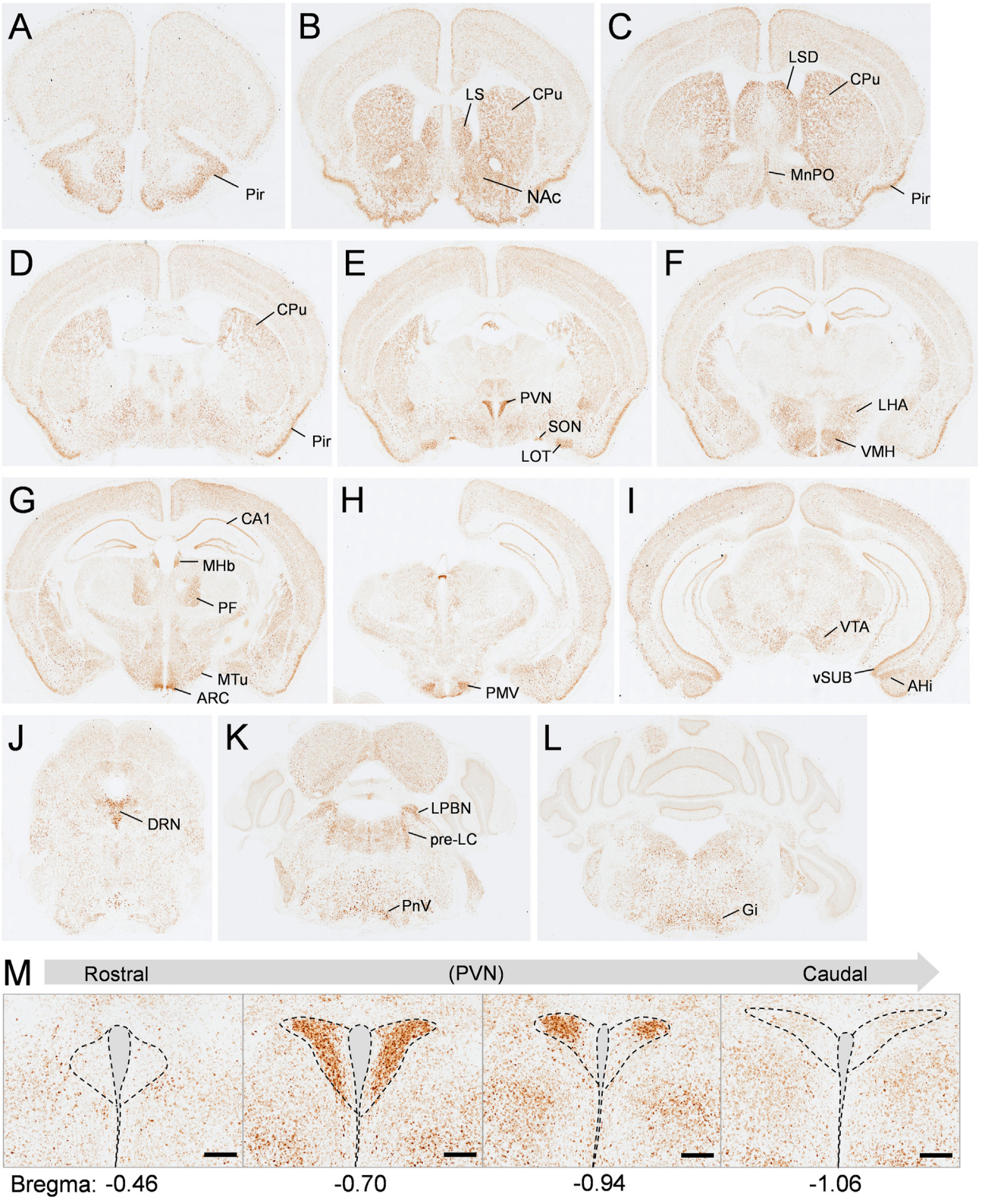


**Figure 1: Broad but regionally enriched Rgs2 mRNA expression in the mouse brain.** (A–L) Whole brain section RNAscope images showing the regionally enriched distribution of *Rgs2* mRNA throughout the brain. Note that brain regions with relatively high expression of *Rgs2* mRNA are denoted. (M) Zoom-in RNAscope images showing *Rgs2* mRNA expression pattern throughout the rostral-caudal PVN. Pir, piriform cortex; LS, lateral septal nucleus; LSD, lateral septal nucleus, dorsal part; NAc, accumbens nucleus; CPu, caudate putamen; PVN, paraventricular nucleus of hypothalamus; SON, supraoptic nucleus; LOT, nucleus of the lateral olfactory tract; LHA, lateral hypothalamic nucleus; VMH, ventromedial nucleus of hypothalamus; CA1, field CA1 of the hippocampus; MHb, medial habenular nucleus; PF, parafascicular thalamic nucleus; ARC, arcuate nucleus of hypothalamus; MTu, medial tuberal nucleus; PMV, ventral premammillary nucleus; VTA, ventral tegmental area; vSUB, ventral subiculum; AHi, amygdalohippocampal area; DRN, dorsal raphe nucleus; LPBN, lateral parabrachial nucleus; pre-LC, pre-locus coeruleus; PnV, ventral pontine reticular nucleus; Gi, gigantocellular reticular nucleus. Scale bar for M, 200 μm.

 

Fluorescent Multiplex assays, slides were mounted and coverslipped with VECTASHIELD HardSet mounting medium (H-1500, Vector Laboratories).

### 2.17. Fluorescent immunohistochemistry (FIHC) and fluorescent nissl staining

Immunohistochemistry was performed as previously reported [24]. Briefly, brain sections were rinsed in PBS, and then incubated in blocking buffer (3% normal donkey serum, 0.3% Triton-X100 in PBS) for 30 min at room temperature. After blocking, the sections were incubated with primary antibodies (1:1000, 3% normal donkey serum, 0.3% Tween-20 in PBS) overnight at 4 °C, then rinsed in 0.3% PBST and incubated with secondary antibodies (1:500, 3% normal donkey serum, 0.3% Tween-20 in PBS) for 1 h at room temperature. Sections were then mounted with VECTASHIELD HardSet mounting medium (H-1500, Vector Laboratories) and coverslipped. For RNAscope ISH and FIHC co-labeling studies, FIHC was performed as described above immediately after RNAscope ISH.

Fluorescent Nissl stain (NeuroTrace 530/615, Invitrogen #N21482) was performed to label PVN neurons. Briefly, after the incubation with secondary antibodies as described above, sections were rinsed in PBS and incubated with NeuroTrace stain (1:500 dilution in PBS) for 30 min at room temperature. Sections were then washed extensively with PBS and mounted with VECTASHIED HardSet mounting medium and coverslipped.

### 2.18. Imaging and quantification

Brain sections were scanned by Olympus Slideview VS200 with bright field microscopy (for RNAscope 2.5 HD Brown assays) or fluorescent microscopy (For RNAscope Fluorescent Multiplex assays and immunofluorescence assays). For the brain *Rgs2* mRNA mapping study, regions of interest were marked by manually drawing the border according to the mouse brain atlas (The Mouse Brain in Stereotaxic Coordinates, Third Edition). To quantify co-expression of *Rgs2*/FG and *Rgs2*/CRH, PVN sections (bregma ∼ -0.8 mm) were selected, PVN border was determined as described above, and $Rgs2^{+}$/$FG^{+}$/$CRH^{+}$ cell-counting and/or co-expression were determined with Fiji (ImageJ) software. The quantification of PVN Nissl $^{+}$ neurons was done similarly as described above. To quantify the relative expression level of *Rgs2* in PVN, PVN sections (bregma ∼ -0.8 mm) were picked from individual animals. Signal intensity of *Rgs2* and DAPI within PVN were determined by Fiji (Image J) software, and the intensity of *Rgs2* was normalized by the intensity of DAPI and compared between the groups.

### 2.19. Data analysis

GraphPad Prism 9 software (GraphPad) and SPSS software (IBM) were used to perform statistical analyses. The differences between two groups were tested with unpaired Student's t tests. Multiple variable comparisons were made by two-way ANOVA, followed by Holm-Sidak multiple comparison procedures. Heat production was corrected using fat-free mass as a covariate via generalized linear model analysis (GLM). A p-value $< 0.05$ was considered to be statistically significant. Data are presented as mean ± SEM.

## 3. RESULTS

### 3.1. Rgs2 mRNA is widely expressed in the mouse brain

It was reported that *Rgs2* mRNA was expressed at moderate to high levels in several rat brain regions using traditional $^{35}$S-UTP-labeled ISH [22]. In order to gain insight into detailed expression patterns of *Rgs2* in the mouse brain, we performed RNAscope ISH [37] on WT mouse brain sections. Varying degrees of *Rgs2* expression was detected across the brain, with relatively enriched *Rgs2* expression being observed in multiple brain regions (Figure 1), including piriform cortex (Pir), nucleus accumbens, lateral septal nucleus (LS), caudate putamen (CPu), median preoptic nucleus (MnPO), PVN, supraoptic nucleus (SON), lateral olfactory tract (LOT), central amygdala (CeA), lateral hypothalamic area (LHA), ventromedial hypothalamic nucleus (VMH), arcuate hypothalamic nucleus (ARC), medial tuberal nucleus (MTu), CA1 of the hippocampus, medial habenular nucleus (MHb), parafascicular thalamic nucleus (PF), premammillary nucleus ventral part (PMV), ventral tegmental area (VTA), ventral subiculum (vSUB), amygdalohippocampal area (AHi), dorsal raphe nucleus (DRN), lateral parabrachial nucleus (LPBN), pre-locus coeruleus (pre-LC), ventral pontine reticular nucleus (PnV), and gigantocellular reticular nucleus (Gi) (Figure 1A-L and Fig. S1A-R). Of note, the PVN appears to be the one with highest *Rgs2* expression among those brain regions and more focused assessment further revealed that *Rgs2* mRNA is uniquely concentrated in the middle, but not rostral or caudal, PVN (Figure 1M).

### 3.2. Rgs2 is enriched in PVN endocrine cells and responds to metabolic stress

The PVN is a key integrative center where distinct neuronal populations differentially regulate metabolic homeostasis, sympathetic control of cardiovascular function, and stress responses [6,7,38,39]. Given the initial observation of enriched expression of *Rgs2* mRNA in the middle PVN where endocrine neurons are mainly located, we further examined whether *Rgs2* is indeed expressed in PVN endocrine neurons. To this end, we performed i. p. Injection of retrograde tracer FG into WT mice as i. p. injection of FG has been validated in previous studies to specifically label PVN endocrine neurons [33–36]. After one week of incubation, the brains were extracted, sectioned, and processed for combined *Rgs2*-RNAscope and FG-FIHC. We observed an impressive overlap between *Rgs2* and FG in the PVN and subsequent quantification revealed that more than 90% of PVN $FG^{+}$ endocrine neurons are also $Rgs2^{+}$ (Figure 2A,B). Corticotrophin-releasing hormone (CRH)-expressing neurons represent one of the major populations of PVN endocrine neurons and therefore, we further performed combined *Rgs2*-RNAscope and CRH-FIHC, which revealed that most (89.6%) $CRH^{+}$ neurons also express *Rgs2* (Figure 2C,D). To further confirm these histological findings, we also conducted *in silico* bioinformatics analysis with publicly available PVN single-cell RNA-seq data (GSE148568) [28]. Consistent with our histological examination, single-cell RNA-seq data analysis revealed that among the 8 clustered PVN *Sim-1*$^{+}$ neuron populations (Figure 2E), *Rgs2* is enriched in putative PVN endocrine neurons, with the highest expression level in $CRH^{+}$ neurons (Figure 2F). It has been shown that PVN CRH neuronal activity and responsiveness are impacted by nutritional states [40,41]. Additionally, previous studies demonstrated that cellular *Rgs2* mRNA level was upregulated in response to various forms of stress [42]. Here, we investigated whether PVN *Rgs2* mRNA expression level can be altered by fasting-induced acute metabolic challenge. Interestingly, RNAscope ISH results demonstrated that *Rgs2* expression was elevated specifically in the PVN, but not the ARC, after 24 h fasting (Figure 2G–I), indicating that *Rgs2* might play a unique role in the adaptive response of PVN endocrine neurons to metabolic challenge.

### 3.3. $Rgs2^{Sim1-KO}$ mice have normal metabolic phenotypes

Despite that $Rgs2^{null}$ mice exhibit reduced body weight, altered adipogenesis and thermoregulation [20] and that Rgs2 mRNA is highly expressed in the PVN, it is unknown if PVN RGS2 contributes to whole-body energy metabolism. Therefore, we generated a novel mouse model

 

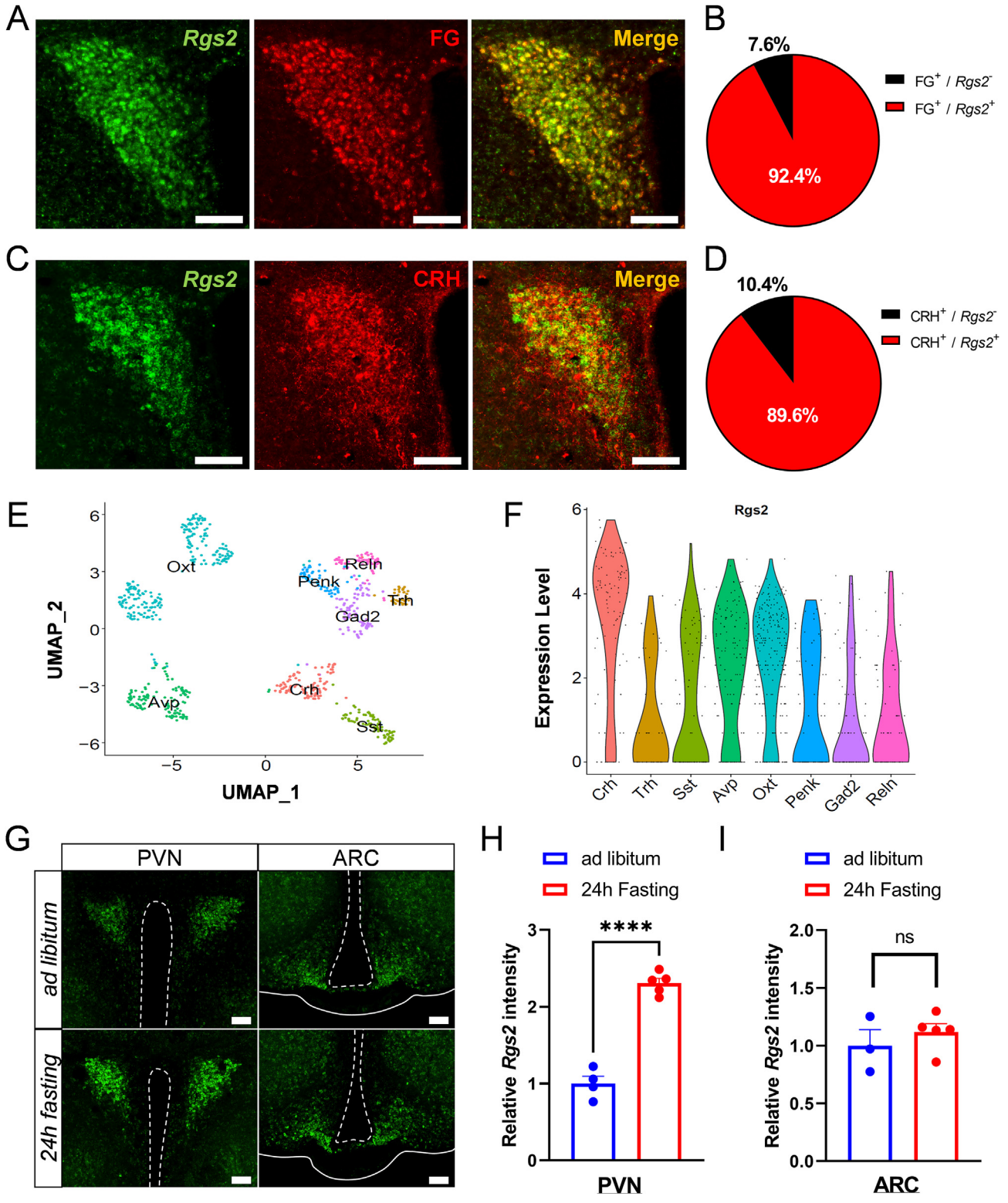


**Figure 2: *Rgs2* mRNA is enriched in PVN endocrine cells and fasting further increases PVN *Rgs2* expression.** (**A**–**D**) Co-labeling of *Rgs2* mRNA with endocrine neurons marked by i. p. Injection of fluorogold (FG) (A, B) or CRH$^{+}$ PVN endocrine neurons (C, D) (N = 3/group). (**E, F**) *In silico* analysis of PVN single-cell RNA-seq database confirmed the enrichment of *Rgs2* mRNA in CRH $^{+}$ putative PVN endocrine neurons. (**G**–**I**) *Rgs2* mRNA expression (G) in the PVN (H), but not in the ARC (I), is increased after 24 h fasting (N = 3–5/group). All scale bars, 100 μm. Data are expressed as mean ± SEM. ****p < 0.0001 (unpaired Student's t test).

 

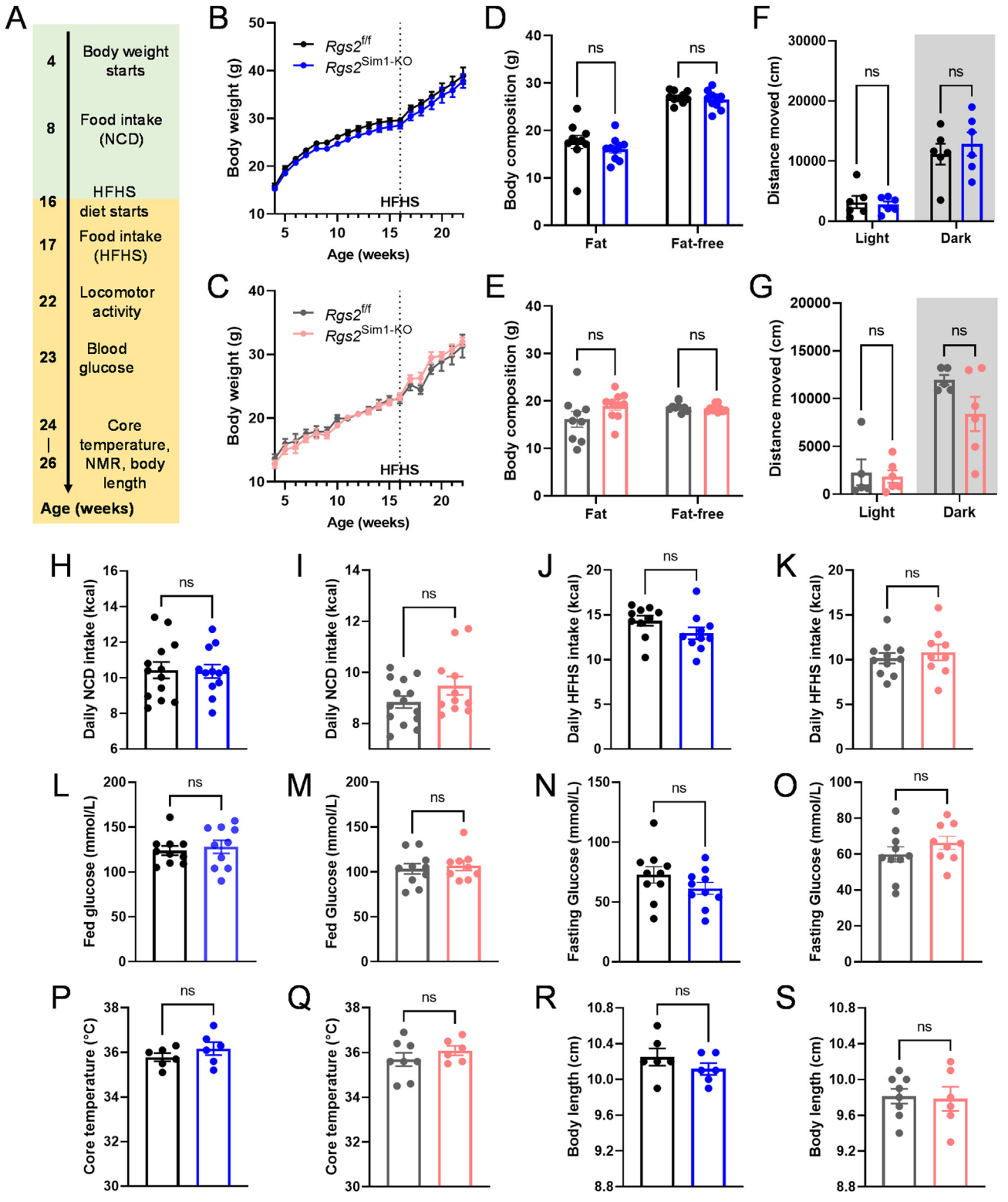


**Figure 3: *Sim1*-Cre mediated prenatal *Rgs2* deletion in the PVN (*Rgs2*$^{Sim1\text{-}KO}$) does not affect metabolic homeostasis.** (**A**) Schematic showing experimental timeline. (**B**–**C**) Body weight growth curve of both male (B) and female (C) *Rgs2*$^{Sim1-KO}$ and control littermates (note that mice were challenged with HFHS diet for 6 weeks from 16 weeks of age; N = 6–12/group). (**D, E**) Body composition (NMR) of male (D) and female (E) *Rgs2*$^{Sim1-KO}$ and control littermates. (**F, G**) Locomotor activity of male (F) and female (G) *Rgs2*$^{Sim1-KO}$ and control littermates in PhenoTyper cages during light and dark phases. (**H, I**) Daily energy intake upon normal chow diet (NCD) feeding in both males (H) and females (I). (**J, K**) Daily energy intake upon HFHS feeding in both males (J) and females (K). (**L-O**) Fed/fasting blood glucose levels at the end of HFHS challenge for both males (L, N) and females (M, O). (**P**–**S**) Core temperature (P, Q) and body length (R, S) for both male (P, R) and female (Q, S) mice. Data are expressed as mean ± SEM. Two-way ANOVA (B–C, F-G) and unpaired Student's t test (D-E, H–S) were performed for statistical analyses.

 

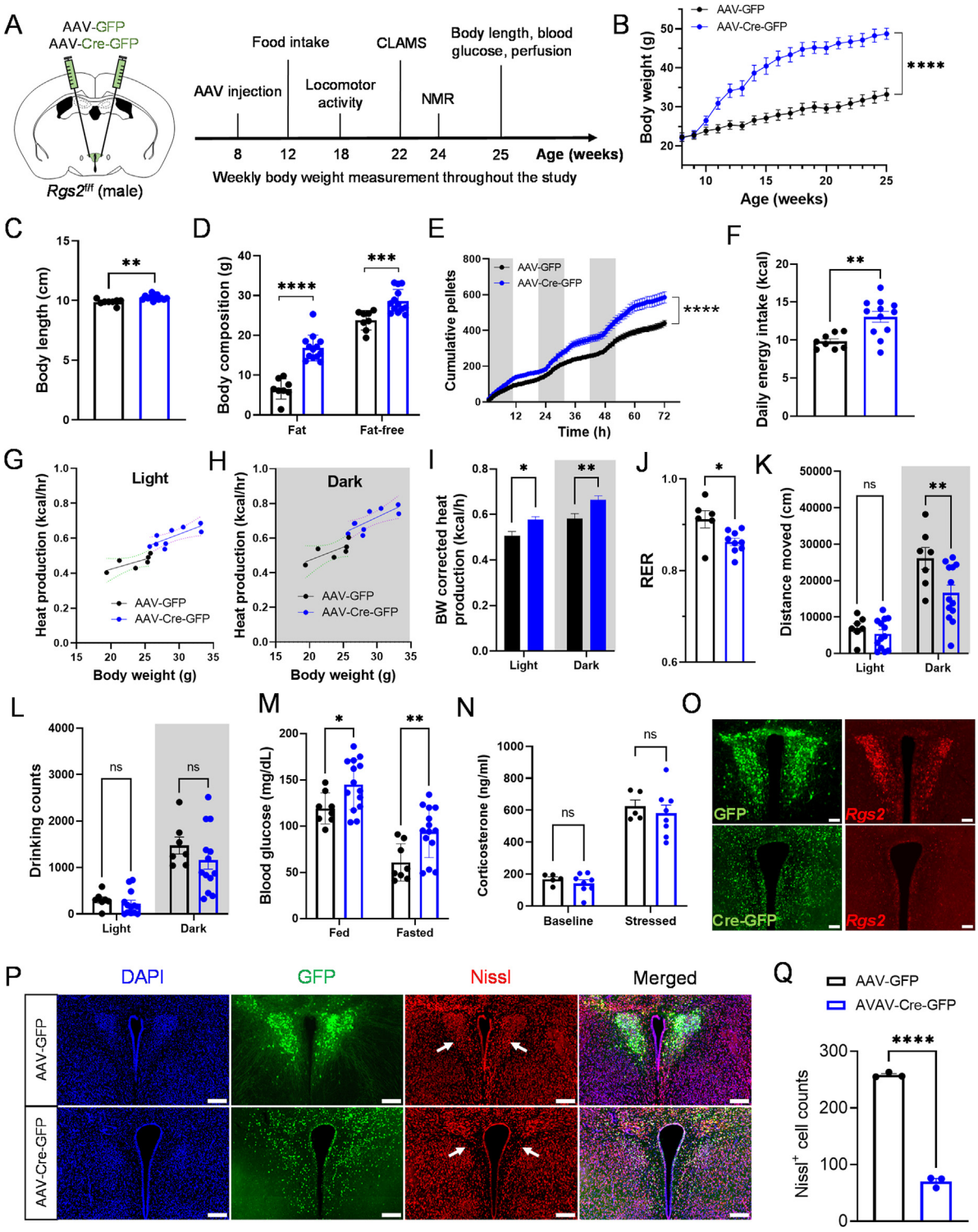


**Figure 4: AAV-mediated postnatal deletion of *Rgs2* in the PVN causes obesity and loss of PVN neurons.** (**A**) Schematic showing AAV injection and experimental timeline. (**B**) Body weight growth curve of male *Rgs2*$^{f/f}$ mice received microinjection of either AAV-GFP or AAV-Cre-GFP into the PVN at 8 weeks of age (N = 8–13/group). (**C, D**) Body length at 25-week-old (C) and body composition measured by NMR at 24-week-old (D). (**E, F**) Accumulative food intake (E) and average daily food intake (F) during 3-day measurement period by FED3 (shaded periods indicate dark phases). (**G-I**) Regression analysis of uncorrected values of hourly heat production versus body mass during light (G) or dark (H) phases and estimated marginal mean values of hourly heat production at FFM covariate value of 26.78 g (I). (**J**) Respiratory exchange ratio (RER) measured in CLAMS cage. (**K, L**) Locomotor activity (K) and drinking behavior (L) measured in PhenoTyper cages during light and dark (shaded) phases. (**M**) Fed/fasted blood glucose measurement at 24-week-old. (**N**) Plasma corticosterone level at baseline and in response to 30 min restraint stress. (**O**) Representative images showing near-absent level of *Rgs2* mRNA expression (by RNAscope) in *Rgs2*$^{f/f}$ mice received microinjection of AAV-Cre-GFP into the PVN. (**P, Q**) Representative images of Nissl staining (O) and quantified result (P) showing the significant loss of PVN neurons in *Rgs2*$^{f/f}$ mice received microinjection of AAV-Cre-GFP into the PVN. Data are expressed as mean ± SEM. *p < 0.05, **p < 0.01, ***p < 0.001, and ****p < 0.0001 b y two-way ANOVA (B, E, K, L-M), unpaired Student's t test (C, D, F, J, P), or GLM analysis (G–I). Scale bars for (O), 100 μm; scale bars for (P), 200 μm.

 

in which *Rgs2* is ablated from *Sim1*-expressing cells ($Rgs2^{Sim1-KO}$) developmentally to evaluate the role of PVN RGS2 in the homeostatic regulation of energy balance. We first attempted to validate an effective deletion of *Rgs2* in the PVN by performing RNAscope FISH, which revealed only a partial knockdown of *Rgs2* FISH signal in $Rgs2^{Sim1-KO}$ mice compared to control $Rgs2^{f/f}$ littermates, whereas *Rgs2* FISH signal is nearly abolished in $Rgs2^{null}$ mice (Fig. S2A). We reasoned this could be due to the production of truncated *Rgs2* mRNA lacking exons 2–4 in the PVN of $Rgs2^{Sim1-KO}$ mice, which can still be recognized and bound to *Rgs2* RNAscope probes to produce FISH signal (albeit with lower level). To test if this is the case, we designed two sets of PCR primer pair spanning either exons 1–5 or exons 2–4 (Fig. S2B) and performed qPCR using cDNA samples prepared from the PVN punches of $Rgs2^{Sim1-KO}$ and $Rgs2^{f/f}$ littermates (Figs. S2C and D). Consistent with our theory, we observed a non-statistically significant increase in *Rgs2* mRNA level in $RGS2^{Sim1-KO}$ mice with exons 1–5 primer pair (Fig. S2C), which we attributed to the more efficient PCR amplification of shortened amplicon in $Rgs2^{Sim1-KO}$ compared to long amplicon in $Rgs2^{f/f}$ littermates (Fig. S2E). In contrast, qPCR with exons 2–4 primer pair using the same cDNA samples showed more than 50% reduction of PVN *Rgs2* mRNA in $Rgs2^{Sim1-KO}$ mice compared to $Rgs2^{f/f}$ littermates (Fig. S2D). Additional qPCR for other RGS family members revealed a trend toward reduced expression of *Rgs*5 and *Rgs*10, but not *Rgs*4, *Rgs*7, *Rgs*12 or *Rgs*17, in $Rgs2^{Sim1-KO}$ mice (Figs. S2F–K).

After the validation of effective deletion of *Rgs2* in the PVN of $Rgs2^{Sim1-KO}$ mice, we carried out a series of metabolic phenotyping studies according to the experimental timeline shown in Figure 3A. To our surprise, both male and female $Rgs2^{Sim1-KO}$ mice showed comparable body weight gain when fed normal chow diet (NCD) or challenged with high-fat high sucrose (HFHS) diet (Figure 3B,C). Body composition (at the end of HFHS challenge), locomotor activity and daily food intake were also comparable between $Rgs2^{Sim1-KO}$ and $Rgs2^{f/f}$ littermates (Figure 3D–K). Likewise, both sexes of $Rgs2^{Sim1-KO}$ exhibited normal fed/fasting glucose levels, core body temperature and body length (Figure 3L–S). Taken together, these results demonstrate that prenatal deletion of *Rgs2* in *Sim1*-expressing cells that include the vast majority of PVN neurons (but not glial cells) [43–45] does not cause metabolic disruptions in mice.

### 3.4. AAV-mediated RGS2 deletion in PVN leads to altered metabolic phenotypes

Developmental compensation for the conditional loss of functionally critical genes is not uncommon for a biological system of an organism. To further investigate whether such a mechanism may occur in $Rgs2^{Sim1-KO}$ mice, we utilized a viral approach to generate mice with postnatal ablation of PVN *Rgs2* and evaluated metabolic consequences. We performed stereotaxic injection of either AAV-GFP or AAV-Cre-GFP (from Addgene) into the PVN of 8-week-old $Rgs2^{f/f}$ mice, followed by a set of metabolic phenotyping studies according to the experimental timeline shown in Figure 4A. In striking contrast to prenatal PVN *Rgs2* deletion in $Rgs2^{Sim1-KO}$ mice, we observed that young adult male $Rgs2^{f/f}$ mice that received AAV-Cre-GFP injection into the PVN ($Rgs2^{PVN-KO}$ mice) quickly gain excess weight as early as 3 weeks after viral injection (Figure 4B). $Rgs2^{PVN-KO}$ mice also exhibited increased body length as measured at the end of the study (Figure 4C). Body composition analysis by NMR revealed that $Rgs2^{PVN-KO}$ mice have increased mass for both fat and fat-free components (more so for fat mass; Figure 4D). Measurement of food intake with Feeding Experimentation Device 3 (FED3) 4 weeks after virus injection showed that $Rgs2^{PVN-KO}$ mice consume more food than control mice (Figure 4E,F). On the other hand, OxyMax/CLAMS metabolic cage studies revealed that compared with control mice, male $Rgs2^{PVN-KO}$ mice have a slight but significantly increased heat production after GLM correction using fat-free mass (FFM) as a covariate (FFM at 26.78 g; Light phase: model $p_l < 0.001$, FFM $p = 0.002$, AAV $p = 0.016$; Dark phase: model $p < 0.001$, FFM $p = 0.002$, AAV $p = 0.023$) (Figure 4G–I). These results indicate that the body weight gain in $Rgs2^{PVN-KO}$ mice is due to increased food intake, but not reduced energy expenditure. In addition, male $Rgs2^{PVN-KO}$ mice showed reduced respiratory exchange ratio (RER) (Figure 4J), suggesting increased fat utilization as an energy resource. $Rgs2^{PVN-KO}$ mice also exhibit reduced locomotor activities in the dark phase without significant changes in drinking behavior (Figure 4K,L). Fed and fasting blood glucose levels were also increased in $Rgs2^{PVN-KO}$ mice (Figure 4M). Surprisingly, despite being obese, the plasma corticosterone level in $Rgs2^{PVN-KO}$ mice was comparable to control mice both at baseline and in response to 30 min restraint stress (Figure 4N). Interestingly, in sharp contrast to considerable residual *Rgs2* RNAscope FISH signal observed in $Rgs2^{Sim1-KO}$ mice, we observed a near-absent level of *Rgs2* RNAscope FISH signal in the PVN of $Rgs2^{PVN-KO}$ mice (Figure 4O), which led us to question whether PVN neurons expressing RGS2 are lost in $Rgs2^{PVN-KO}$ mice. To test this possibility, we performed Nissl staining to visualize and quantify PVN neurons. Results highlighted a significant loss of PVN neurons in $Rgs2^{PVN-KO}$ mice (Figure 4P, Q). Importantly, nearly identical metabolic phenotypes and PVN neuronal loss were observed in female $Rgs2^{PVN-KO}$ mice (Figs. S3A–K).

While AAV vectors expressing Cre recombinase are widely used to achieve conditional gene manipulations for functional investigation, it is worth noting that excessive Cre expression can lead to off-target effects in certain cell types and brain regions [46,47]. To rule out the possibility that the metabolic phenotypes observed in $Rgs2^{PVN-KO}$ mice were due to such cytotoxicity of Cre itself rather than Cre-mediated *Rgs2* deletion, we injected AAV-GFP and AAV-Cre-GFP (Addgene) into the PVN of 8-week-old WT mice (Figure 5A). Weekly body weight monitoring revealed that Cre-GFP expression alone in WT mice does not cause significant body weight gain within 5 weeks of viral injection, whereas $Rgs2^{f/f}$ mice receiving Cre-GFP gained significant body weight within this timeframe (Figure 5B,C). Additionally, Nissl staining of brain sections at this timepoint after viral delivery also showed that both WT and $Rgs2^{f/f}$ mice receiving AAV-Cre-GFP injection retain normal PVN structure and a comparable number of PVN neurons to that of AAV-GFP injected WT mice (Figure 5D,E). Taken together, these results indicate that at least the initial body weight gain of $Rgs2^{PVN-KO}$ mice within 5 weeks post-AAV is not due to Cre-GFP expression itself and is independent of PVN neuronal loss.

### 3.5. Metabolic phenotypes induced by AAV-mediated PVN Rgs2 deletion in young adult mice can be recapitulated in older adult mice

To further confirm the effect of AAV-mediated PVN *Rgs2* deletion on body weight homeostasis, we injected an independently developed set of AAV-Cre-GFP and AAV-GFP vectors from a different vendor (UNC vector core) into the PVN of 18-week-old $Rgs2^{f/f}$ and WT mice. Consistent with what we observed in young $Rgs2^{PVN-KO}$ mice described above, both male and female older $Rgs2^{PVN-KO}$ mice also exhibited significantly increased body weight 4 weeks after virus injection (Figure 6B,C, E, F). Further, NMR body composition analysis revealed that body weight gain in both sexes of older $Rgs2^{PVN-KO}$ mice was due to increases in both fat and fat-free mass (Figure 6D,G). Importantly, neither body weight nor body composition was altered by AAV-Cre-GFP injection in older male WT mice (Figure 6H–J), which again indicates that phenotypes observed in older $Rgs2^{PVN-KO}$ mice were not due to the potential Cre cytotoxicity. Taken together, these results confirmed that AAV-mediated postnatal deletion of PVN *Rgs2*

 

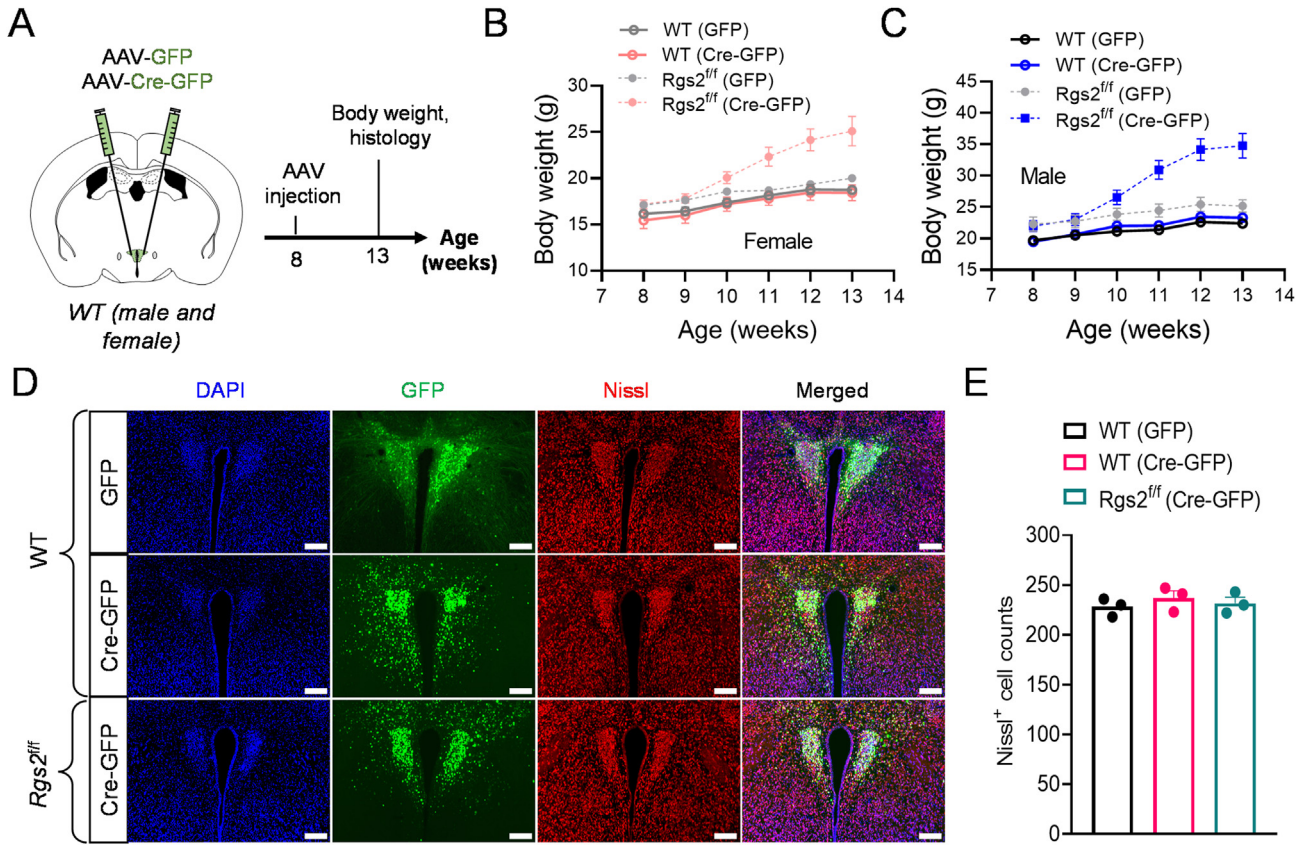


**Figure 5: Body weight gain after 4–5 weeks of AAV-Cre-GFP injection into the PVN of *Rgs2*$^{f/f}$ mice is not due to the potential cytotoxicity of Cre or PVN neuronal loss.** **(A)** Schematic showing AAV injection and experimental timeline. **(B, C)** Weekly body weight growth curve after microinjection of AAVs into the PVN of 8-week-old female **(B)** and male (C) WT mice; note that *Rgs2*$^{f/f}$ received microinjection of either AAV-GFP or AAV-Cre-GFP into the PVN (from Figure 3B and Fig. S3B) were plotted together (dashed line) to indicate body weight gain only in *Rgs2*$^{f/f}$ received AAV-Cre-GFP injection (WT, N = 3–5/group; *Rgs2*$^{f/f}$, N = 7–13/group). **(D, E)** Representative FIHC images (D) and the quantification of PVN neurons (Nissl) (E) after 5 weeks of AAV injection in female mice (N = 3/group). Data are expressed as mean ± SEM. All scale bars = 200 μm.

readily disrupts metabolic homeostasis in mice, regardless of vector source or animal age.

## 4. DISCUSSION

Much is known about the importance of GPCR signaling pathways within the PVN for the homeostatic regulation of energy balance, yet downstream molecular mediators of these signaling pathways that affect metabolic homeostasis remain largely unknown. In the present study, we provide the first evidence to show that RGS2, a member of subfamily B/R4 RGS proteins, is enriched in PVN endocrine neurons and affects metabolic homeostasis.

Despite reduced body weight and impaired adipogenesis have been reported in global *Rgs2*$^{null}$ mice [17,20], in the present study, we found that mice lacking *Rgs2* in the PVN postnatally (*Rgs2*$^{PVN\text{-}KO}$), but not prenatally (*Rgs2*$^{Sim1-KO}$), are prone to weight gain, implying a rather complex spatiotemporal role of RGS2 in energy balance control. Opposing metabolic phenotypes in whole-body *Rgs2*$^{Null}$ and *Rgs2*$^{PVN\text{-}KO}$ strongly suggest that peripheral and central actions of RGS2 are likely antagonistic to the regulation of energy balance. Additionally, the complete absence of metabolic phenotypes in *Rgs2*$^{Sim1-KO}$ indicates that developmental loss of PVN RGS2 can be compensated by yet unknown mechanisms. One such mechanism could be the compensatory increase of other closely functionally relevant RGS members in the PVN, such as RGS4 [48,49]. We indeed examined some other RGS members expressed in the PVN but did not observe an increase in any of those RGS members. However, it remains possible that other RGS members that were not tested could still compensate for the developmental loss of Rgs2 in the PVN. Critically, in addition to a difference in temporal resolution (postnatal versus prenatal ablation of PVN *Rgs2*), other differences also exist between *Rgs2*$^{PVN\text{-}KO}$ and *Rgs2*$^{Sim1-KO}$ mouse models. First, although *Sim1*-Cre line has been frequently used for conditional gene manipulations in the PVN, Cre recombinase activity in extra-PVN regions, such as the medial amygdala and the nucleus of lateral olfactory tract (LOT), has also been reported [50]. In fact, we also generated *Sim1*-Cre/tdTomato reporter mice and observed a rather broad distribution of tdTomato + cells across the brain than previously reported, including some hypothalamic nuclei known to be important for metabolic control, such as dorsomedial nucleus and lateral hypothalamic area (unpublished observation). Thus, it remains to be seen if *Rgs2* deletion in those extra-PVN brain regions of *Rgs2*$^{Sim1-KO}$ mice somehow offset the phenotypic appearance of PVN *Rgs2* deletion. Second, it should be noted that Cre expression in *Sim1*-Cre mouse is likely limited to neurons but not glial cells [44,51], while viral-mediated *Rgs2* deletion in *Rgs2*$^{PVN\text{-}KO}$ could have affected glial cells as we used AAV serotype 2 that expresses Cre-GFP under the CMV promoter [52]. *Rgs2* seems to be expressed in glial cells such as astrocytes and microglia [53], and studies have shown that glial cells are also involved in the regulation of energy balance [54,55]. Thus, it is conceivable that in *Rgs2*$^{PVN\text{-}KO}$ mice, *Rgs2* was deleted not only in

 

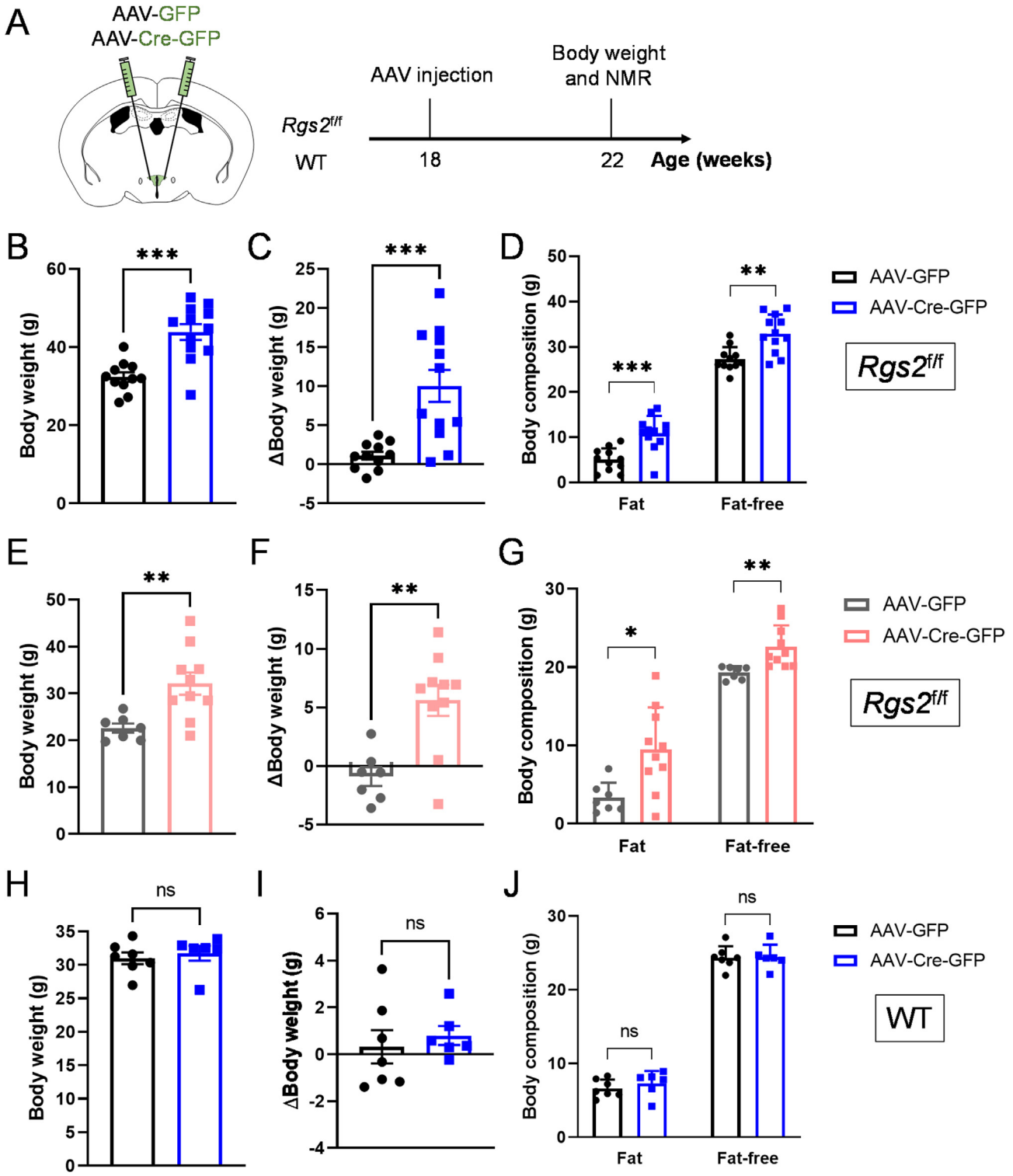


**Figure 6: AAV-mediated postnatal deletion of *Rgs2* in the PVN causes weight gain in mature adult mice.** (**A**) Schematic showing AAV injection and experimental timeline. (**B-G**) Absolute body weight (B, E), changes in body weight (C, F) and NMR body composition (D, G) after 4 weeks of AAV-GFP or AAV-Cre-GFP microinjection into the PVN of 18-week-old male (B–D) and female (E–G) *Rgs2*$^{f/f}$ mice. (**H-J**) Absolute body weight (H), changes in body weight (I) and NMR body composition (J) after 4 weeks of AAV-GFP or AAV-Cre-GFP microinjection into the PVN of 18-week-old male WT mice. Data are expressed as mean ± SEM. *p < 0.05, **p < 0.01, ***p < 0.001 b y student's t test.

neurons but also in glia cells residing in the PVN; however, the impact of *Rgs2* deletion in those PVN glia cells on energy balance remains unknown. Further studies using AAV vectors expressing Cre recombinase under neuron-, astrocyte- or microglia-specific promoters would help to determine the relative contribution of *Rgs2* in each of these PVN cell types for metabolic control.

 

One striking observation in the present study is the loss of PVN neurons in *Rgs2*$^{PVN\text{-}KO}$ mice. There is a perceived concern that the death of PVN neurons could be due to Cre cytotoxicity rather than Cre-mediated PVN *Rgs2* deletion [46,47], which could have significantly contributed to the rapid weight gain in *Rgs2*$^{PVN\text{-}KO}$ mice after viral injection [50,56]. However, the results of our control experiments did not support this possibility, as AAV-Cre-GFP injection into the PVN of WT mice did not cause significant weight gain compared to that of AAV-GFP control group after 5 weeks of AAV injection, whereas *Rgs2*$^{PVN\text{-}KO}$ mice gained significantly more weight by then. Interestingly, Nissl staining at 5 weeks of post-AAV showed a comparable number of PVN neurons in either WT or *Rgs2*$^{f/f}$ mice received AAV-Cre-GFP injection to that of WT mice received AAV-GFP injection, indicating that at least the initial rapid weight gain observed in *Rgs2*$^{PVN\text{-}KO}$ mice was not due to the significant loss of PVN neurons. However, the presence of PVN neurons visualized with Nissl staining by no means implies these neurons are functionally intact, and how might the adult loss of *Rgs2* affect the functionality of PVN endocrine neurons is of great interest for future investigations. From what has been reported in the literatures regarding the functional role of RGS2, the impact of postnatal *Rgs2* deletion brought to the physiology of PVN endocrine neurons could be multifaceted. It has been shown that RGS2 not only functions as a GAP to directly terminate $G_{\alpha q}$ and/or $G_{\alpha i}$ signaling but also indirectly blocks $G_{\alpha s}$ signaling by directly binding to and inhibiting adenylyl cyclase in various cell types [13,15,57,58]. Unfortunately, however, neither the relative selectivity of RGS2 towards different $G_{\alpha}$ subunits nor the GPCRs affected by RGS2 specifically in PVN endocrine neurons has been explored. Additionally, it has also been shown that RGS2 could affect cellular functions independently of GPCR-$G_{\alpha}$ signaling by acting as a regulator of protein translational process or different ion channel activities [59,60]. Collectively, these seemingly diverse functionalities of RGS2 warrant future in-depth studies to uncover the mechanism of action of RGS2 within PVN endocrine neurons for metabolic homeostasis.

The PVN contains many neurochemically and functionally distinct neuronal populations [61,62], which enable the diverse functionalities of PVN neurons ranging from endocrine stress response, metabolic homeostasis, to sympathetic control of cardiovascular function [6,7,38,39]. Accordingly, the activity of PVN neurons is highly responsive to behavioral and physiological challenges as demonstrated by the expression of immediate early genes (IEGs), such as c-Fos, after exposure to diverse forms of emotional stress or metabolic challenge [63]. Our observation of a more than 2-fold increase of *Rgs2* mRNA expression in the PVN after 24 h fasting is interesting because it suggests that RGS2 might function as an important mediator of neuroendocrine responses upon calorie restriction. Fasting has been shown to activate PVN CRH$^{+}$ neurons and increase plasma corticosterone levels [64–67], it will be of interest to evaluate HPA axis activity in *Rgs2*$^{PVN\text{-}KO}$ mice under various metabolic challenges. Another interesting observation is that the induction of *Rgs2* by 24 h fasting seems to be limited to the PVN as we did not observe such increases in the ARC, a brain region known to be highly sensitive to body energy status and critical for metabolic control [68]. One potential explanation is that increase in PVN *Rgs2* in response to 24 h fasting could be due to distress caused by extreme hunger rather than caloric deficit per se. However, *Rgs2*$^{PVN\text{-}KO}$ mice appear to have normal HPA axis activation in response to restraint stress as plasma corticosterone levels were comparable between the *Rgs2*$^{PVN\text{-}KO}$ and control mice. Nonetheless, future studies are warranted to clarify the roles of PVN *Rgs2* in other behavioral and physiological responses to different types of stress.

## 5. CONCLUSION

In summary, we identified RGS2 as a PVN endocrine neuron-enriched signaling modulator whose expression level is sensitive to metabolic challenge. Functionally, our results demonstrated an indispensable role of PVN RGS2 in the regulation of metabolic homeostasis when ablated postnatally. Given the importance of hypothalamic GPCR signaling pathways for the development of anti-obesity medications as well as the known role of RGS2 in modulating GPCR-$G_{\alpha}$ signaling, our findings support RGS2 as a potential molecular candidate which could be targeted to develop a novel therapeutic approach for obesity.

## AUTHOR CONTRIBUTIONS

YD, JLG, and HC contributed to conceptualization, study design, methodology, and manuscript writing. JED, KS, GD, US, JJ, BAT, ZZ, and LVZ conducted and assisted the experiments. YD, JMR, and HC contributed to the data analysis.

## DATA AVAILABILITY

Data will be made available on request.

## ACKNOWLEDGMENTS

This work was supported by grants from the National Institutes of Health (HL127673 and HL084207 to HC; HL134850, DK133121, HL084207, and UL1TR001436 to JLG), and the American Heart Association (19POST34450083 to US; 19POST34380239 and T32DK112751 to GD).

## CONFLICT OF INTEREST

The authors declare no conflict of interest.

## APPENDIX A. SUPPLEMENTARY DATA

Supplementary data to this article can be found online at https://doi.org/10.1016/j.molmet.2022.101622.

## REFERENCES

[1] Loos, R.J.F., Yeo, G.S.H., 2022. The genetics of obesity: from discovery to biology. Nat Rev Genet 23(2):120–133.
[2] Myers Jr., M.G., Affinati, A.H., Richardson, N., Schwartz, M.W., 2021. Central nervous system regulation of organismal energy and glucose homeostasis. Nat Metab 3(6):737–750.
[3] Rui, L., 2013. Brain regulation of energy balance and body weight. Rev Endocr Metab Disord 14(4):387–407.
[4] Schwartz, M.W., Porte Jr., D., 2005. Diabetes, obesity, and the brain. Science 307(5708):375–379.
[5] Muller, T.D., Bluher, M., Tschop, M.H., DiMarchi, R.D., 2022. Anti-obesity drug discovery: advances and challenges. Nat Rev Drug Discov 21(3):201–223.
[6] Atasoy, D., Betley, J.N., Su, H.H., Sternson, S.M., 2012. Deconstruction of a neural circuit for hunger. Nature 488(7410):172–177.
[7] Qin, C., Li, J., Tang, K., 2018. The paraventricular nucleus of the hypothalamus: development, function, and human diseases. Endocrinology 159(9):3458–3472.

 

[8] Sutton, A.K., Myers Jr., M.G., Olson, D.P., 2016. The role of PVH circuits in leptin action and energy balance. Annu Rev Physiol 78:207–221.

[9] Deng, Y., Deng, G., Grobe, J.L., Cui, H., 2021. Hypothalamic GPCR signaling pathways in cardiometabolic control. Front Physiol 12:691226.

[10] Chen, M., Berger, A., Kablan, A., Zhang, J., Gavrilova, O., Weinstein, L.S., 2012. Gsalpha deficiency in the paraventricular nucleus of the hypothalamus partially contributes to obesity associated with Gsalpha mutations. Endocrinology 153(9):4256–4265.

[11] Li, Y.Q., Shrestha, Y., Pandey, M., Chen, M., Kablan, A., Gavrilova, O., et al., 2016. G(q/11)alpha and G(s)alpha mediate distinct physiological responses to central melanocortins. J Clin Invest 126(1):40–49.

[12] Stewart, A., Fisher, R.A., 2015. Introduction: G protein-coupled receptors and RGS proteins. Prog Mol Biol Transl Sci 133:1–11.

[13] Masuho, I., Balaji, S., Muntean, B.S., Skamangas, N.K., Chavali, S., Tesmer, J.J.G., et al., 2020. A global map of G protein signaling regulation by RGS proteins. Cell 183(2):503–521 e19.

[14] Osei-Owusu, P., Blumer, K.J., 2015. Regulator of G Protein signaling 2: a versatile regulator of vascular function. Prog Mol Biol Transl Sci 133:77–92.

[15] Sinnarajah, S., Dessauer, C.W., Srikumar, D., Chen, J., Yuen, J., Yilma, S., et al., 2001. RGS2 regulates signal transduction in olfactory neurons by attenuating activation of adenylyl cyclase III. Nature 409(6823):1051–1055.

[16] Gross, V., Tank, J., Obst, M., Plehm, R., Blumer, K.J., Diedrich, A., et al., 2005. Autonomic nervous system and blood pressure regulation in RGS2-deficient mice. Am J Physiol Regul Integr Comp Physiol 288(5):R1134–R1142.

[17] Klepac, K., Yang, J., Hildebrand, S., Pfeifer, A., 2019. RGS2: a multifunctional signaling hub that balances brown adipose tissue function and differentiation. Mol Metabol 30:173–183.

[18] Mark, M.D., Wollenweber, P., Gesk, A., Kosters, K., Batzke, K., Janoschka, C., et al., 2019. RGS2 drives male aggression in mice via the serotonergic system. Commun Biol 2:373.

[19] McNabb, H.J., Zhang, Q., Sjogren, B., 2020. Emerging roles for regulator of G protein signaling 2 in (Patho)physiology. Mol Pharmacol 98(6):751–760.

[20] Nunn, C., Zhao, P., Zou, M.X., Summers, K., Guglielmo, C.G., Chidiac, P., 2011. Resistance to age-related, normal body weight gain in RGS2 deficient mice. Cell Signal 23(8):1375–1386.

[21] Tank, J., Obst, M., Diedrich, A., Brychta, R.J., Blumer, K.J., Heusser, K., et al., 2007. Sympathetic nerve traffic and circulating norepinephrine levels in RGS2-deficient mice. Auton Neurosci 136(1–2):52–57.

[22] Grafstein-Dunn, E., Young, K.H., Cockett, M.I., Khawaja, X.Z., 2001. Regional distribution of regulators of G-protein signaling (RGS) 1, 2, 13, 14, 16, and GAIP messenger ribonucleic acids by in situ hybridization in rat brain. Brain Res Mol Brain Res 88(1–2):113–123.

[23] Osei-Owusu, P., Sabharwal, R., Kaltenbronn, K.M., Rhee, M.H., Chapleau, M.W., Dietrich, H.H., et al., 2012. Regulator of G protein signaling 2 deficiency causes endothelial dysfunction and impaired endothelium-derived hyperpolarizing factor-mediated relaxation by dysregulating Gi/o signaling. J Biol Chem 287(15):12541–12549.

[24] Cui, H., Sohn, J.W., Gautron, L., Funahashi, H., Williams, K.W., Elmquist, J.K., et al., 2012. Neuroanatomy of melanocortin-4 receptor pathway in the lateral hypothalamic area. J Comp Neurol 520(18):4168–4183.

[25] Singh, U., Jiang, J., Saito, K., Toth, B.A., Dickey, J.E., Rodeghiero, S.R., et al., 2022. Neuroanatomical organization and functional roles of PVN MC4R pathways in physiological and behavioral regulations. Mol Metabol 55:101401.

[26] Schmittgen, T.D., Livak, K.J., 2008. Analyzing real-time PCR data by the comparative C(T) method. Nat Protoc 3(6):1101–1108.

[27] Saito, K., Davis, K.C., Morgan, D.A., Toth, B.A., Jiang, J., Singh, U., et al., 2019. Celastrol reduces obesity in MC4R deficiency and stimulates sympathetic nerve activity affecting metabolic and cardiovascular functions. Diabetes 68(6):1210–1220.

[28] Xu, S., Yang, H., Menon, V., Lemire, A.L., Wang, L., Henry, F.E., et al., 2020. Behavioral state coding by molecularly defined paraventricular hypothalamic cell type ensembles. Science 370(6514).

[29] Hao, Y., Hao, S., Andersen-Nissen, E., Mauck 3rd, W.M., Zheng, S., Butler, A., et al., 2021. Integrated analysis of multimodal single-cell data. Cell 184(13):3573–3587 e29.

[30] Grobe, J.L., 2017. Comprehensive assessments of energy balance in mice. Methods Mol Biol 1614:123–146.

[31] Reho, J.J., Nakagawa, P., Mouradian Jr., G.C., Grobe, C.C., Saravia, F.L., Burnett, C.M.L., et al., 2022. Methods for the comprehensive in vivo analysis of energy flux, fluid homeostasis, blood pressure, and ventilatory function in rodents. Front Physiol 13:855054.

[32] Ye, Y., Abu El Haija, M., Morgan, D.A., Guo, D., Song, Y., Frank, A., et al., 2020. Endocannabinoid receptor-1 and sympathetic nervous system mediate the beneficial metabolic effects of gastric bypass. Cell Rep 33(4):108270.

[33] Gasparini, S., Resch, J.M., Narayan, S.V., Peltekian, L., Iverson, G.N., Karthik, S., et al., 2019. Aldosterone-sensitive HSD2 neurons in mice. Brain Struct Funct 224(1):387–417.

[34] Merchenthaler, I., 1991. Neurons with access to the general circulation in the central nervous system of the rat: a retrograde tracing study with fluoro-gold. Neuroscience 44(3):655–662.

[35] Eliava, M., Melchior, M., Knobloch-Bollmann, H.S., Wahis, J., da Silva Gouveia, M., Tang, Y., et al., 2016. A new population of parvocellular oxytocin neurons controlling magnocellular neuron activity and inflammatory pain processing. Neuron 89(6):1291–1304.

[36] Luther, J.A., Daftary, S.S., Boudaba, C., Gould, G.C., Halmos, K.C., Tasker, J.G., 2002. Neurosecretory and non-neurosecretory parvocellular neurones of the hypothalamic paraventricular nucleus express distinct electrophysiological properties. J Neuroendocrinol 14(12):929–932.

[37] Wang, F., Flanagan, J., Su, N., Wang, L.C., Bui, S., Nielson, A., et al., 2012. RNAscope: a novel in situ RNA analysis platform for formalin-fixed, paraffin-embedded tissues. J Mol Diagn 14(1):22–29.

[38] Herman, J.P., Tasker, J.G., 2016. Paraventricular hypothalamic mechanisms of chronic stress adaptation. Front Endocrinol 7:137.

[39] Nunn, N., Womack, M., Dart, C., Barrett-Jolley, R., 2011. Function and pharmacology of spinally-projecting sympathetic pre-autonomic neurones in the paraventricular nucleus of the hypothalamus. Curr Neuropharmacol 9(2):262–277.

[40] Melnick, I., Krishtal, O.A., Colmers, W.F., 2020. Integration of energy homeostasis and stress by parvocellular neurons in rat hypothalamic paraventricular nucleus. J Physiol 598(5):1073–1092.

[41] Zhu, C., Xu, Y., Jiang, Z., Tian, J.B., Cassidy, R.M., Cai, Z.L., et al., 2020. Disrupted hypothalamic CRH neuron responsiveness contributes to diet-induced obesity. EMBO Rep 21(7):e49210.

[42] Nguyen, C.H., Zhao, P., Sobiesiak, A.J., Chidiac, P., 2012. RGS2 is a component of the cellular stress response. Biochem Biophys Res Commun 426(1):129–134.

[43] Fan, C.M., Kuwana, E., Bulfone, A., Fletcher, C.F., Copeland, N.G., Jenkins, N.A., et al., 1996. Expression patterns of two murine homologs of Drosophila single-minded suggest possible roles in embryonic patterning and in the pathogenesis of Down syndrome. Mol Cell Neurosci 7(1):1–16.

[44] Michaud, J.L., Rosenquist, T., May, N.R., Fan, C.M., 1998. Development of neuroendocrine lineages requires the bHLH-PAS transcription factor SIM1. Genes Dev 12(20):3264–3275.

[45] Balthasar, N., Dalgaard, L.T., Lee, C.E., Yu, J., Funahashi, H., Williams, T., et al., 2005. Divergence of melanocortin pathways in the control of food intake and energy expenditure. Cell 123(3):493–505.

[46] Janbandhu, V.C., Moik, D., Fassler, R., 2014. Cre recombinase induces DNA damage and tetraploidy in the absence of loxP sites. Cell Cycle 13(3):462–470.


 

[47] Rezai Amin, S., Gruszczynski, C., Guiard, B.P., Callebert, J., Launay, J.M., Louis, F., et al., 2019. Viral vector-mediated Cre recombinase expression in substantia nigra induces lesions of the nigrostriatal pathway associated with perturbations of dopamine-related behaviors and hallmarks of programmed cell death. J Neurochem 150(3):330–340.

[48] Barbaric, I., Miller, G., Dear, T.N., 2007. Appearances can be deceiving: phenotypes of knockout mice. Briefings Funct Genomics Proteomics 6(2):91–103.

[49] Doupnik, C.A., 2015. RGS redundancy and implications in GPCR-GIRK signaling. Int Rev Neurobiol 123:87–116.

[50] Nyamugenda, E., Trentzsch, M., Russell, S., Miles, T., Boysen, G., Phelan, K.D., et al., 2019. Injury to hypothalamic Sim1 neurons is a common feature of obesity by exposure to high-fat diet in male and female mice. J Neurochem 149(1):73–97.

[51] Kublaoui, B.M., Holder Jr., J.L., Gemelli, T., Zinn, A.R., 2006. Sim1 haploinsufficiency impairs melanocortin-mediated anorexia and activation of paraventricular nucleus neurons. Mol Endocrinol 20(10):2483–2492.

[52] O'Carroll, S.J., Cook, W.H., Young, D., 2020. AAV targeting of glial cell types in the central and peripheral nervous system and relevance to human gene therapy. Front Mol Neurosci 13:618020.

[53] Tabula Muris Consortium, 2018. Single-cell transcriptomics of 20 mouse organs creates a Tabula Muris. Nature 562(7727):367–372.

[54] Argente-Arizon, P., Guerra-Cantera, S., Garcia-Segura, L.M., Argente, J., Chowen, J.A., 2017. Glial cells and energy balance. J Mol Endocrinol 58(1): R59–R71.

[55] Nampoothiri, S., Nogueiras, R., Schwaninger, M., Prevot, V., 2022. Glial cells as integrators of peripheral and central signals in the regulation of energy homeostasis. Nat Metab 4(7):813–825.

[56] Leibowitz, S.F., Hammer, N.J., Chang, K., 1981. Hypothalamic paraventricular nucleus lesions produce overeating and obesity in the rat. Physiol Behav 27(6): 1031–1040.

[57] Roy, A.A., Baragli, A., Bernstein, L.S., Hepler, J.R., Hebert, T.E., Chidiac, P., 2006. RGS2 interacts with Gs and adenylyl cyclase in living cells. Cell Signal 18(3):336–348.

[58] Zhang, Q., Haak, A.J., Sjogren, B., 2022. Regulator of G protein signaling 2 inhibits Galphaq-dependent uveal melanoma cell growth. J Biol Chem 298(6): 101955.

[59] Nguyen, C.H., Ming, H., Zhao, P., Hugendubler, L., Gros, R., Kimball, S.R., et al., 2009. Translational control by RGS2. J Cell Biol 186(5):755–765.

[60] Schoeber, J.P., Topala, C.N., Wang, X., Diepens, R.J., Lambers, T.T., Hoenderop, J.G., et al., 2006. RGS2 inhibits the epithelial Ca2+ channel TRPV6. J Biol Chem 281(40):29669–29674.

[61] Simmons, D.M., Swanson, L.W., 2009. Comparison of the spatial distribution of seven types of neuroendocrine neurons in the rat paraventricular nucleus: toward a global 3D model. J Comp Neurol 516(5):423–441.

[62] Stern, J.E., 2001. Electrophysiological and morphological properties of preautonomic neurones in the rat hypothalamic paraventricular nucleus. J Physiol 537(Pt 1):161–177.

[63] Kovacs, K.J., 2008. Measurement of immediate-early gene activation- c-fos and beyond. J Neuroendocrinol 20(6):665–672.

[64] Akana, S.F., Strack, A.M., Hanson, E.S., Dallman, M.F., 1994. Regulation of activity in the hypothalamo-pituitary-adrenal axis is integral to a larger hypothalamic system that determines caloric flow. Endocrinology 135(3): 1125–1134.

[65] Sainsbury, A., Zhang, L., 2012. Role of the hypothalamus in the neuroendocrine regulation of body weight and composition during energy deficit. Obes Rev 13(3):234–257.

[66] Li, C., Navarrete, J., Liang-Guallpa, J., Lu, C., Funderburk, S.C., Chang, R.B., et al., 2019. Defined paraventricular hypothalamic populations exhibit differential responses to food contingent on caloric state. Cell Metabol 29(3): 681–694 e5.

[67] Kim, J., Lee, S., Fang, Y.Y., Shin, A., Park, S., Hashikawa, K., et al., 2019. Rapid, biphasic CRF neuronal responses encode positive and negative valence. Nat Neurosci 22(4):576–585.

[68] Joly-Amado, A., Cansell, C., Denis, R.G., Delbes, A.S., Castel, J., Martinez, S., et al., 2014. The hypothalamic arcuate nucleus and the control of peripheral substrates. Best Pract Res Clin Endocrinol Metabol 28(5):725–737.

 